Catalysis Science & Technology

ROYAL SOCIETY OF CHEMISTRY

PAPER

View Article Online
View Journal | View Issue

Cite this: *Catal. Sci. Technol.*, 2025, **15**, 3216

Experimental and computational optimisation of methanol dehydration to dimethyl ether†

Maciej G. Walerowski, [a] Stylianos Kyrimis, [b] Matthew E. Potter, [c] Alice E. Oakley, [a] Marina Carravetta, [a] Lindsay-Marie Armstrong [b] and Robert Raja *[a]

Received 17th January 2025,
Accepted 2nd April 2025

DOI: 10.1039/d5cy00062a

rsc.li/catalysis

Meeting the International Maritime Organization's net-zero target by 2050 necessitates the replacement of marine fossil fuels with sustainable alternatives, such as dimethyl ether (DME). Silicon-doped aluminophosphate (SAPO) solid acid catalysts, particularly the weakly-acidic SAPO-11, can catalyse the selective dehydration of methanol-to-DME with exceptional stability. Herein, we present a combined experimental, computational fluid dynamics, and design of experiments study to augment catalyst efficiency and DME production, and to support scale-up endeavours. Using a four-dimensional design surface, it was found that longer catalyst beds and higher operating temperature increase DME yields, with the catalyst bed length having a more pronounced influence. In contrast, the use of highly concentrated methanol reactant streams had a detrimental effect and this was ascribed to a saturation of the active sites in the SAPO-11 catalyst. Improved single-pass conversions and catalyst longevity on industrial scales can thus be achieved by optimising both the number of acid sites in SAPO-11 and reaction parameters.

Introduction

International shipping accounted for 2% of global CO_2 emissions in 2022,[1] which may swell to 13% in a few decades.[2] Electrification of long haul maritime shipping is currently challenging due to the low energy density of batteries, highlighting the need for sustainable and energy dense fuels.[3–5] Although methanol and ammonia are currently being explored as alternative fuels for the marine sector,[6–8] dimethyl ether (DME) may be more promising. DME is non-toxic, compatible with a circular carbon economy, and can be readily integrated into existing liquid petroleum gas infrastructure which enables its rapid deployment as a sustainable marine fuel.[9–12]

DME can be produced either *via* methanol dehydration, or the one-pot conversion of CO_2 *via* a methanol intermediate,[9–13] with both methods requiring an acidic catalyst. The traditional methanol-to-DME (MTD) γ-Al_2O_3 catalyst is rapidly deactivated by water produced during the reaction.[10,12,14] In contrast, microporous aluminosilicate solid acid catalysts not only impart shape and size selectivity to this reaction, but are also less susceptible to water-induced deactivation than γ-Al_2O_3.[15] However, aluminosilicates possess strong Brønsted acid sites (BAS) which facilitate the methanol-to-olefins (MTO) reaction and coke formation, thus reducing DME selectivity and catalyst stability.[9,12,16,17]

Aluminophosphates (AlPOs) and silicon-doped aluminophosphates (SAPOs) form similar frameworks to aluminosilicates. Whilst aluminosilicates frameworks are based on vertex-sharing tetrahedral AlO_4 and SiO_4 species, AlPOs form near identical frameworks, based on alternating AlO_4 and PO_4 tetrahedra. Incorporating silicon into the AlPO framework generates a range of possible acid sites, depending on whether silicon substitutes a phosphorous atom (type II), or an aluminium-phosphorous pair (type III). This leads to the formation of either isolated BAS (type II) or silicon islands with BAS located on the periphery of these islands (type III).[18–20] Bonding in SAPOs is more ionic compared to aluminosilicates,[21] resulting in stronger interactions between the acidic protons and conjugate-basic framework oxygens which reduces their acid strength and makes SAPOs auspicious for the MTD reaction.[18,22] SAPO-11 is a particularly promising candidate for the selective production of DME, as silicon substitutes into the AlPO-11 framework primarily *via* type III substitution, forming silicon islands which reduces the overall acidity.[22–26] When applied for MTD, SAPO-11 can achieve 100% DME selectivity, and retain consistent activity even up to 200 hours' on-stream.[22] This is likely due to the favourable combination of weakly acidic sites which cannot facilitate the competing MTO reaction, and

[a] *School of Chemistry and Chemical Engineering, University of Southampton, Southampton, SO17 1BJ, UK. E-mail: R.Raja@soton.ac.uk*
[b] *School of Engineering, University of Southampton, Southampton, SO17 1BJ, UK*
[c] *Department of Chemistry, University of Bath, Bath, BA2 7AY, UK*
† Electronic supplementary information (ESI) available. See DOI: https://doi.org/10.1039/d5cy00062a

medium-sized channels which spatially constrain the formation of bulky coke precursors.[27] In contrast, at comparable temperatures, H-ZSM-5 yielded 95% DME selectivity.[28] Thus, the use of SAPO-11 as a MTD catalyst could translate to a vast reduction in waste and separation costs on an industrial scale.

To accelerate the implementation of SAPO-11 as a MTD catalyst, the macroscopic behaviour must be modelled to facilitate process optimisation. Computational fluid dynamics (CFD) can model the macroscopic behaviour of fluid flowing through a fixed bed reactor by solving a series of mass, momentum, and energy conservation equations, whilst incorporating species mass exchange from chemical reactions.[29] CFD simulations additionally facilitate parametric investigations *in silico*, without the need for multiple costly experiments. This is beneficial for scale-up as detrimental phenomena, such as hotspot formation and pressure drop, can be identified and proactively managed which can potentially minimise catalyst deactivation and maximise productivity. Through an extensive parametric study, Kyrimis *et al.* highlighted the benefit of using CFD to improve the industrial reactor design for the CO_2-to-methanol reaction. They calculated that using a CFD-optimised reactor design, methanol productivity could be increased by 6.9% with a 75% lower pressure drop, compared to a baseline reactor.[30] CFD modelling can also provide a unique macroscale view of a reaction by demonstrating the local variations in velocity, pressure, density, temperature, and species concentrations inside a catalytic bed. Potter *et al.* used CFD to investigate catalytic ethanol dehydration over SAPO-34, highlighting the link between operating temperature, spatial variations in species concentration within the catalyst bed, and the location of the associated cold- and hotspots.[31] In a similar vein, Zhuang *et al.* modelled the MTO reaction over SAPO-34 on an industrial scale, with a particular focus on the dynamic nature of the reaction in the temporal dimension.[32] CFD simulations showed that the deactivation front moves from the catalyst bed inlet to the outlet as the reaction proceeds with time. The observed inverse relationship between methanol conversion and space velocity was attributed to lower residence times in the catalyst bed at higher space velocities. Kyrimis *et al.* used CFD to test two different kinetic models for the CO_2-to-methanol reaction,[33] showing that although both kinetic models gave similar outlet gas compositions, the temperature profiles inside the catalyst bed varied significantly depending on the kinetic model used. This is a key finding for validation of kinetic models as these are usually derived using only the outlet species concentrations. Incorrect information regarding the species distribution within a catalytic bed could misinform engineering decisions. Thus, a reliable kinetic model must also account for the species distribution along the bed to ensure its accuracy. This type of insight afforded by CFD modelling is challenging to obtain experimentally as it requires bespoke reactors, and even then, the nature of the measurement itself can influence the results. As such, CFD modelling can provide unique and complementary insights which can support scale-up.

In this work, we present a combined experimental and computational optimisation of the MTD reaction using SAPO-11. We firstly investigate the influence of reaction parameters such as temperature, catalyst granule size, methanol concentration in the inlet stream, catalyst bed length, and active site abundance, on experimental catalytic performance. This data then informs the development of kinetic and CFD models, providing a unique and complementary macroscale insight which enables further process optimisation. To the best of our knowledge, this is the first study of its kind which combines empirical studies, fully validated CFD modelling, and design of experiments (DoE) investigations to bridge multiple scales and provide valuable information for scale-up of the solid acid catalysed MTD reaction.

Experimental

Catalyst synthesis and characterisation

SAPO-11 (Si/Al ratio of 0.20) catalyst was synthesised by modifying a hydrothermal procedure from Murthy *et al.*,[34] and this was used to understand the influence of temperature, catalyst granule size, catalyst bed length, and reactant gas stream methanol concentration on the MTD reaction. As a follow-up investigation, the procedure outlined by Murthy *et al.*[34] was initially used to synthesise additional SAPO-11 catalysts with different silicon loadings to explore the influence of BAS abundance on catalytic performance. However, phase impurities were found when the Si/Al ratio was lowered below 0.20. As such, an alternative hydrothermal procedure outlined by Grenev *et al.*[35] was modified to obtain four SAPO-11 catalysts with varying silicon loadings (intended Si/Al ratio between 0.05–0.20) for the follow-up investigation. The catalysts are termed SAPO-11(x) whereby x is the silicon loading in wt%. The full synthetic protocols for these catalysts are described in section 1 of the ESI.† The two types of catalysts are discussed in isolation as they have been synthesised using two different methods for distinct applications and as such are not directly comparable.

The catalysts were thoroughly characterised using energy dispersive spectroscopy (EDS), powder X-ray diffraction (XRD), surface area and porosity analysis, scanning electron microscopy (SEM), solid state nuclear magnetic resonance (ssNMR), ammonia temperature programmed desorption (NH_3-TPD), and carbon hydrogen nitrogen (CHN) analysis. The full details of these techniques can be found in section 2 of the ESI.†

Catalytic testing

SAPO-11 solid acid catalysts were tested for the MTD reaction in a fixed bed, continuous flow reactor (Fig. S1†) at atmospheric pressure. Outlet gases were analysed in triplicate using a PerkinElmer Clarus 480 gas chromatograph employing a 30 m, 0.25 mm, 0.25 μm Elite-5 column, a 30 °C isothermal temperature programme, and a flame ionisation detector. All experiments were performed in triplicate using a fresh catalyst on separate days in a randomised order and the standard deviation between the repeats is presented as an error bar. Each data point is therefore the combination of nine independent GC injections.

SAPO-11 powder was firstly compressed at 4 tonnes for 10 seconds as this was found to yield minimal framework porosity degradation.[36] As per the approach outlined by Kyrimis *et al.*,[37] the resulting pellet was then crushed and sieved five times to yield catalyst granules in the size range of 106–300, 300–500, or 500–710 μm. To validate our kinetic model, it is important to understand the distribution of species through the catalyst bed, thus three loadings of SAPO-11 catalyst granules (0.150, 0.300, or 0.450 g), corresponding to three catalyst bed lengths (1.9, 3.6, and 5.4 cm, respectively) were used, similar to Wilkinson *et al.*[38] SAPO-11 catalyst granules of desired size fraction and bed length were then tested at 170, 185, 200, 215, and 230 °C. Methanol at weight hourly space velocities (WHSV) of 0.5, 1, 2, or 3 h^{-1} (based on 0.300 g catalyst loading) was carried into the reactor using nitrogen at flow rates of 41, 38, 31, or 25 mL min^{-1}. Nitrogen carrier gas was varied to maintain consistent total flow rate and hence residence time at the different methanol WHSVs. Further information on the catalytic procedure can be found in section 3 of the ESI.†

Kinetic and computational models

The MTD reaction was modelled using a first-order kinetic model. The experimental data was used to generate apparent rate constants (k) at a range of temperatures and methanol WHSVs using Copasi.[39] Initial estimation of k was performed using a genetic algorithm with a population size of 2000 and 100 generations,[40] followed by a Levenberg–Marquardt local optimisation.[41,42] Apparent activation energy and pre-exponential factors were extracted from a plot of $\ln(k)$ *vs.* $1/T$ and the four values obtained for different methanol WHSV were averaged to give an overall value for the MTD reaction over SAPO-11.

A three-dimensional porous medium CFD model was built in Ansys Fluent 19.2.[43] The cylindrical catalyst bed (0.2 cm radius and 1.9, 3.6, or 5.4 cm height) was meshed with Ansys Meshing to give 700 000 hexahedral computational cells to ensure mesh independency. The computational cell size was 90 μm for a 106–300 μm catalyst granule with a 40% porosity. To replicate the complex nature of the catalytic phenomena, user defined functions were introduced, focused on coupling molecular diffusion (bulk diffusion mechanisms) with molecule-catalyst interactions (Knudsen diffusion mechanism). A modified Arrhenius equation was used within the model to account for active site abundance and occupancy in SAPO-11.[29] Diffusion was described by the dusty-gas model as per Kyrimis *et al.*,[33] inertial and viscous resistances were calculated using the Ergun equation,[44] and de Klerk's correlation was utilised to model axial bed porosity.[45] CFD simulations were performed for 4000 iterations or until convergence was reached, whichever came first.

Results obtained from CFD-driven DoE investigations were modelled using the Sartorius MODDE® 13.1 Pro software suite.[46]

Further details of the kinetic, CFD, and DoE models can be found in sections 4, 5, and 6 of the ESI,† respectively.

Results and discussion

Catalyst characterisation

The SAPO-11 synthesised as per the modified approach from Murthy *et al.*[34] was found to have a Si loading of 2.7 wt% by EDS (Table S1†), hence is now referred to as SAPO-11(2.7). Characterisation of SAPO-11(2.7), described in detail in section 7.1 of the ESI† (Fig. S2–S4 and Tables S1–S3), confirmed the exclusive formation of the intended AEL topology. This concluded that SAPO-11(2.7) was suitable for exploring the influence of reaction parameters on DME yields, and to derive kinetic, CFD, and DoE models.

Four additional SAPO-11 catalysts, with varying silicon loadings (Table S4†), were successfully synthesised using a modified version of the method outlined by Grenev *et al.*[35] These are now referred to as SAPO-11(x) where x represents their actual silicon loading (1.1–2.0 wt%). Characterisation of these four SAPO-11 samples, described in section 7.2 of the ESI† (Fig. S5–S11 and Tables S4–S7), showed that increasing silicon loading primarily increases the number of BAS generated and the total surface area. The SAPO-11 (1.1–2.0) catalysts were used to study the combined influence of BAS abundance and surface area on DME yields.

Catalysis

To accurately determine kinetic parameters, a reaction must be performed in the absence of diffusion limitations and catalyst deactivation.[47] As per the method outlined by Bartholomew and Farrauto,[47] the catalyst granule size was varied (Fig. 1a) to confirm the process was not diffusion limited. DME was the only product observed under all reaction conditions, resulting in a >99.9% DME selectivity. As such, DME percentage yields are equivalent to methanol percentage conversions. Fig. 1a shows no statistically significant differences between the 106–300, 300–500, or 500–710 μm SAPO-11(2.7) granule size fractions under these conditions, in line with findings from Pop *et al.* who also confirmed the absence of internal diffusion limitations for MTD over SAPO-34 granules <1.5 mm in size.[48] Stability testing of SAPO-11(2.7) with 106–300 μm fractions was performed under accelerated deactivation conditions (275 °C, methanol WHSV of 3 h^{-1}), revealing no decrease in catalytic activity after 6 hours' time-on-stream (Fig. 1b), confirming the stability of SAPO-11(2.7) in line with findings reported by Dai *et al.*[22] Overall, this confirmed the suitability of the reaction conditions, and catalyst, for estimating kinetic parameters.

To gain a preliminary insight into the macroscale behaviour of SAPO-11(2.7) for the MTD reaction, the catalyst bed length was varied between 1.9, 3.6, and 5.4 cm, at temperatures between 170 to 230 °C, with a consistent methanol WHSV of 2 h^{-1}. As expected, longer catalyst beds (5.4 cm) gave higher DME percentage yields (Fig. 2) due to increased catalyst amounts. However, diminishing returns were observed with an increase in temperature and no additional DME percentage yields were obtained by

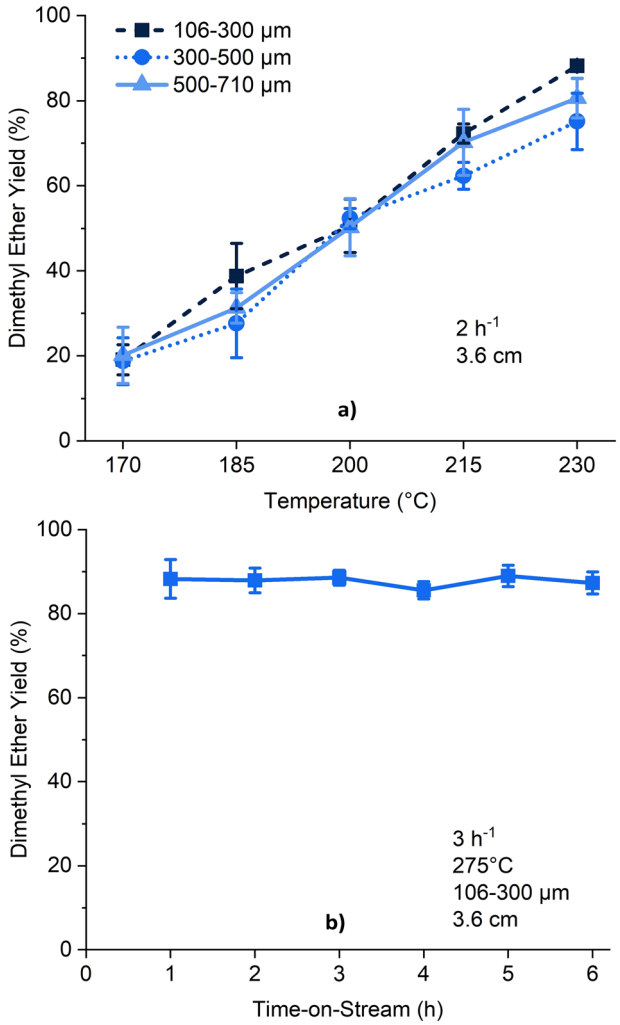

Fig. 1 a) Influence of granule size on catalytic performance at a range of temperatures and b) time-on-stream stability of SAPO-11(2.7).

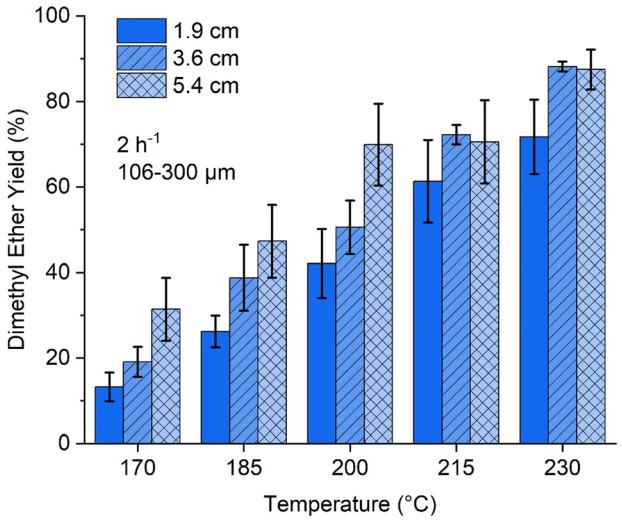

Fig. 2 Impact of SAPO-11 (2.7) catalyst bed length on catalytic performance at a range of temperatures.

lengthening the catalyst bed beyond 3.6 cm above 215 °C. The 3.6 and 5.4 cm beds have practically identical DME percentage yields at 215 and 230 °C, suggesting that maximum DME percentage yields have been reached under these operating conditions. Remarkably, halving the catalyst bed from 3.6 to 1.9 cm does not halve the DME percentage yields. At 170 °C, the 1.9 cm bed gave a 13% DME yield, whereas the 3.6 cm bed produced a 19% DME yield. At 230 °C, the 1.9 and 3.6 cm beds produced DME yields of 72 and 88%, respectively. This indicates that most of the reaction occurs at the inlet to the catalyst bed. Increasing the reaction temperature, speeds up the reaction rate. In doing so, the catalytic activity occurs earlier still in the reaction bed, thereby limiting the influence of extending the bed length under these operating conditions. A 3.6 cm catalyst bed was selected going forward, as it maximised DME percentage yields while keeping catalytic quantities appropriate.

The SAPO-11(2.7) catalysed MTD reaction was performed at a range of methanol WHSVs (0.5, 1, 2, and 3 h^{-1}) and temperatures (170–230 °C) to obtain meaningful data necessary for the development of kinetic models, and to determine temperature and concentration dependencies. To isolate the influence of methanol WHSV on catalytic performance, the nitrogen carrier gas flow was varied, so that the total gas flow (methanol plus nitrogen) was similar, leading to comparable residence times. Associated calculations for this procedure can be found in section 3 of the ESI.† Fig. 3a shows that increasing methanol WHSV leads to a reduction in observed DME percentage yields. Inverse correlations were observed at all temperatures between the methanol WHSV and observed DME percentage yields (Fig. 3b).

Given that the residence time was comparable across all experiments, this was tentatively attributed to a saturation of the SAPO-11 catalyst at higher methanol WHSVs. To test this hypothesis, a follow up investigation was conducted in which the catalytic performance of the four additional SAPO-11 catalysts with a range of silicon loadings (Table S4†) was tested. As previously stated, the only notable difference between these four catalysts was the number of acid sites and the total surface area, enabling direct comparison between the four catalysts. A high methanol WHSV (3 h^{-1}) was used to ensure that any saturation was prominent. Fig. S12† shows that higher DME percentage yields can be attained by doping more silicon into the AlPO-11 framework to give SAPO-11 catalysts more acid sites, but as discussed in section 7.2 of the ESI† and shown by Fig. S5,† this is challenging as silicon does not substitute easily into the AlPO-11 framework. This investigation has shown that there is a correlation between DME percentage yields and active site abundance and accessibility which supports our initial assumption that reduction in observed DME percentage yields at higher methanol WHSVs is due to catalyst saturation.

As seen previously in Fig. 1b, no significant decrease in catalytic activity was observed during an accelerated deactivation study suggesting minimal catalyst deactivation. However, it is unreasonable to assume a complete lack of deactivation. Spent SAPO-11(2.7) catalysts were thus

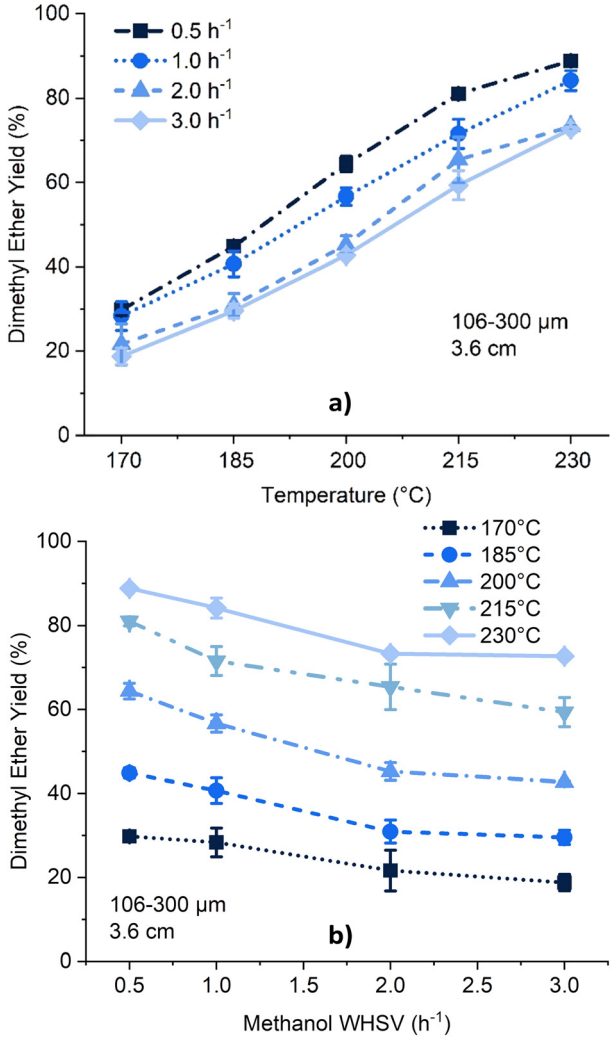

Fig. 3 a) Influence of methanol weight hourly space velocity and temperature on SAPO-11(2.7) catalytic performance. b) A replot of Fig. 3a showing an inverse correlation between methanol weight hourly space velocity and DME yields at a range of temperatures.

characterised to determine the exact level of deactivation occurring. During methanol dehydration, microporous solid acid catalysts deactivate primarily due to the formation of polymeric carbonaceous species (coke) which plug framework pores and thus restrict access to acid sites.[14,17,49–51] CHN analysis was performed to ascertain the precise level of coking and hence deactivation of SAPO-11(2.7) during the MTD reaction. As seen in Table 1, some coking and therefore deactivation has occurred during the MTD reaction. The largest 500–710 μm catalyst granules coke the most and this is ascribed to longer reactant residence times within larger granules which increases the likelihood of further methanol dehydration reactions and coke formation.[51] Increasing methanol WHSV increases coking, and this is due to the catalyst processing a larger volume of reactant feedstock which naturally results in increased coking. For industrial applications, the use of smaller catalyst granules and less concentrated feedstock streams may improve catalyst longevity and hence reduce downtime and maximise productivity. The relationship between coking and silicon loading of SAPO-11 is less clear (Table S8†), with the SAPO-11(1.4) catalyst showing the highest coke formation which is surprising. More work should be done to understand this finding, but this lies outside the scope of this investigation. Reactivation of the SAPO-11 catalyst could be achieved *via* oxidative treatment at 600 °C.[51] For the industrial methanol-to-gasoline process over a H-ZSM-5 catalyst, parallel reactors are used to facilitate regular coke burn-off,[17] vindicating this regeneration strategy on an industrial scale. The coking levels observed within this study (~1 wt%) match those observed by Dai *et al.* who used SAPO-11 for the MTO reaction (0.7 wt%).[52] These levels are significantly lower compared to other catalysts, such as SAPO-34 and SAPO-41, which gain 10.2 and 5.5 wt% of coke during the same reaction.[52] In a separate study, Dai *et al.* showed that SAPO-11 can maintain methanol conversions >85% for as long as 200 hours' on-stream,[22] further confirming the stability of SAPO-11. Compared to other industrially-relevant catalysts such as H-ZSM-5, our SAPO-11 catalyst demonstrates smaller decrease in activity with time-on-stream (Fig. S13†), which validates the excellent stability of SAPO-11 as an MTD catalyst and shows that the small levels of coking seen have no significant influence on observed catalyst performance.

Kinetics

Linear correlations (Fig. 4) were observed between methanol concentrations in the inlet reactant stream and the outlet moles of DME at all temperatures which indicates that the reaction adheres to first-order kinetics.

Table 1 Carbon content of fresh and spent SAPO-11(2.7) catalysts determined using CHN analysis showing the influence of reaction parameters on the amount of coke gained by SAPO-11(2.7) catalysts during methanol dehydration

Methanol WHSV (h^{-1})	Particle size (μm)	Fresh catalyst (wt%)	Spent catalyst (wt%)	Carbon gain (wt%)
2	500–710	0.15 ± 0.09	1.01 ± 0.04	0.86
	300–500	0.09 ± 0.03	0.73 ± 0.01	0.64
	106–300	0.04 ± 0.00	0.73 ± 0.01	0.69
3	106–300	0.04 ± 0.00	1.64 ± 0.02	1.60
2			1.04 ± 0.01	1.00
1			0.84 ± 0.02	0.80
0.5			0.54 ± 0.01	0.50

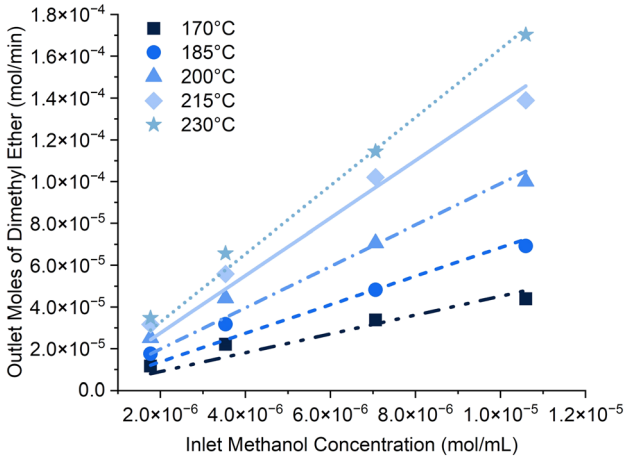

Fig. 4 Linear correlation observed between methanol concentration in the inlet reactant gas stream and the production of DME at a range of temperatures.

This agrees with results reported for methanol dehydration over aluminosilicate catalysts.[53,54] A first-order rate equation was thus used to model methanol dehydration over SAPO-11(2.7) and highly linear correlations were obtained between $\ln(k)$ and $1/T$ at all methanol WHSVs (Fig. S14†). Fig. 1a has already indicated that the reaction is performed in the kinetically-limited regime and the lack of deviations from a straight line further verifies that secondary contributions from any diffusion and/or mass transfer limitations are negligible and hence can be disregarded. The activation energy and pre-exponential factor values were similar for the four methanol WHSVs (Table S9†) and as such they were averaged to give kinetic parameters outlined in Table 2.

Our calculated activation energy is in relatively good agreement with those reported by Catizzone *et al.* for the MTD reaction over aluminosilicates,[53] adding confidence to our findings. To the best of our knowledge, we present for the very first-time kinetic parameters which describe the MTD reaction over SAPO-11 catalysts.

Table 2 Derived kinetic parameters for methanol dehydration over SAPO-11(2.7)

Parameter	Value
Rate equation	Rate = k[methanol]
Kinetic constant equation	$k = \mathrm{Ar/Si_{avail}}$
Ar	$Ae^{\left(-\frac{E_a}{RT}\right)}$
$\mathrm{Si_{Avail}}$	$\left(\frac{A_{cat}}{V_{cat}}\right)^2 Z_k$
Kinetic constants	0.17 to 1.78 s^{-1}
Pre-exponential factor	9.97×10^5 s^{-1}
Activation energy	55.7 kJ mol^{-1}

Where Rate is rate of reaction, k is reaction rate coefficient, [methanol] is methanol concentration, A is pre-exponential factor, E_a is activation energy, R is universal gas constant, T is temperature, A_{cat} is catalyst surface area, V_{cat} is catalyst volume, and Z_k is active site surface coverage with its influence described in eqn (S7) and (S8).†

Computational fluid dynamics

Our kinetic parameters (Table 2) were integrated into a CFD model. Fig. 2 and 3, and S12† have shown that DME yields are influenced by the catalyst bed length, methanol WHSV, and the number of acid active sites in SAPO-11, respectively. We have therefore used a modified Arrhenius equation to account for the limited active site availability in SAPO-11, and hence enable our CFD model to replicate the experimentally-observed dependencies. Fig. 5 and S15 and S16† verify that the CFD model can reproduce temperature, concentration, and catalyst bed length dependencies and accurately predict the outlet mass fractions of all species. The average absolute difference between experimental and CFD outlet mass fractions for all species is 12% which verifies the model accuracy. In line with experimental findings (Fig. S12†), our CFD model is also able to replicate the influence of silicon loading on DME yields (Fig. S17†), whereby SAPO-11 catalysts with a higher silicon loadings can convert a higher

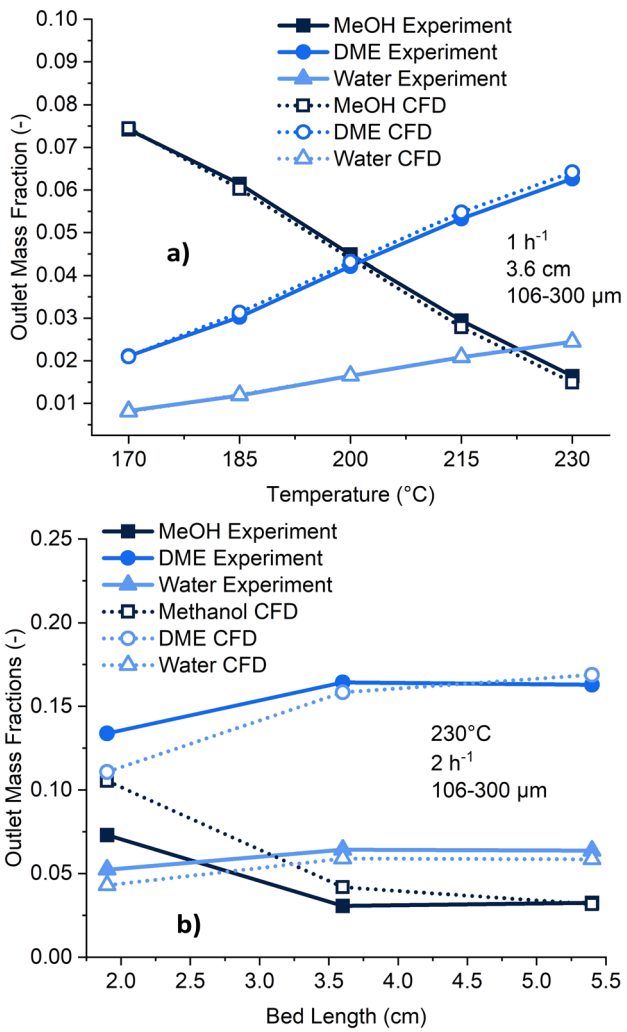

Fig. 5 Comparison between experimental SAPO-11(2.7) and CFD-predicted outlet mass fractions of different species for different a) temperatures and b) catalyst bed lengths.

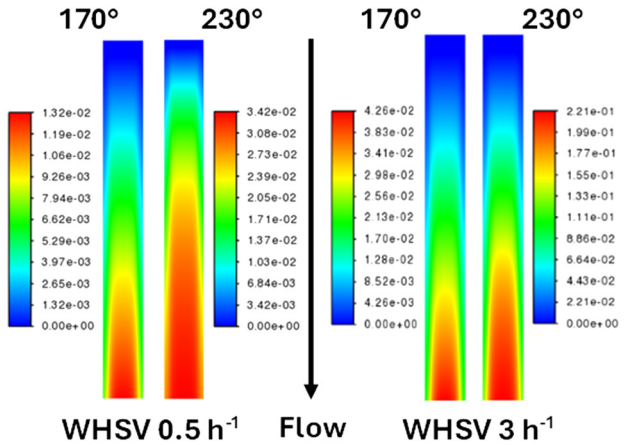

Fig. 6 Two-dimensional contour plots showing the distribution of DME inside the SAPO-11(2.7) catalyst bed at two different temperatures and methanol WHSVs. The values in the legend are the dimensionless mass fractions of DME. Catalyst bed length of 3.6 cm.

percentage of methanol-to-DME. Our thorough validation studies have ensured that the derived kinetics and modelling approach realistically reproduce the reaction behaviour and the involved phenomena throughout the catalyst bed. This yields credibility to the unique insights afforded by CFD and vindicates the use of CFD for further optimisation studies.

Fig. S18† shows that the highest rate of DME production takes place in the inlet half of the catalyst bed. Increasing temperature from 170 to 230 °C causes the maximum rate of DME production to occur earlier still in the catalyst bed which is in line with experimental findings (Fig. 2). Fig. 6 and S19, and S20† show the distribution of DME, water, and methanol in the catalyst bed as a function of temperature and methanol WHSV. Increasing temperature leads to maximum concentrations of DME and water occurring earlier in the catalyst bed, whereas increasing the methanol WHSV leads to maximum concentrations of DME and water occurring later in the catalyst bed. This demonstrates that longer catalyst beds may be required to maximise single-pass methanol conversions at higher methanol WHSVs. Fig. S21† shows that static pressure inside the catalyst bed reduces from the inlet to the outlet. Increasing temperature leads to an increase in static pressure but does not impact the distribution of pressure inside the bed. These unique insights into macroscale phenomena obtained using CFD are challenging to obtain experimentally but can prove vital when scaling up reactions as reactors must be designed to withstand various phenomena within them.

Our CFD model is based on laboratory-scale experiments which were free of appreciable mass transfer and diffusion limitations, and catalyst deactivation, as shown by Fig. 1. In an industrial setting however, the presence of feedstock contaminants can lead to catalyst fouling, and larger scales can exacerbate any mass transfer and diffusion limitations, reducing catalyst activity and longevity. Further refinements to our model could thus be achieved by incorporating results from larger scale pilot plant trials which would confirm the presence and magnitude of any deleterious effects, such as catalyst fouling.

Design of experiment

Validated CFD models not only complement macroscale flow insights under operating conditions but also enable efficient *in silico* simulations of reactions. These parametric studies offer critical insights into operating conditions, guiding engineering decisions to optimize chemical processes. Here, a DoE approach was used to maximise single-pass conversion over a SAPO-11 catalyst as this can improve overall productivity by reducing the need for outlet gas recycling. Data from fifteen additional cases (Fig. S22†), with a variety of temperatures (245–275 °C), catalyst bed lengths (2.5–7.5 cm), and methanol WHSVs (4–6 h^{-1}), was generated using our developed CFD model, and used to inform the DoE study. Again, any change in methanol flow resulted in a concomitant change in nitrogen carrier gas flow to ensure comparable total fluid flow, and similar residence times. The in-depth validation of our CFD model verified that that the influence of parameters such as the operating temperature, catalyst bed length, and methanol concentration on DME yields are accurately understood. As such, we have confidence in exploring beyond the experimental space already investigated. The obtained results were further processed using the Sartorius MODDE® software suite.[46] The software fitted the CFD-derived results using a multiple linear regression approach to give a model with a relative standard deviation of 7%. Four-dimensional contour plots were obtained which succinctly exhibit the influence of catalyst bed length, methanol WHSV, and temperature on methanol conversion (equivalent to DME yield given that as already stated the selectivity was >99.9%).

The aim of the DoE study was to maximise single-pass methanol conversions, and Fig. 7 shows that increasing methanol WHSV leads to a reduction in predicted methanol conversions. This can be attributed to a saturation of the catalyst bed. At a methanol WHSV of 6 h^{-1} (Fig. 7c), the DoE model estimated that highest conversions can only be achieved by simultaneously increasing both the reaction temperature and catalyst bed length. On the other hand, at a methanol WHSV of 4 h^{-1} (Fig. 7a), it is possible to obtain highest predicted conversions, even at low temperatures of 245 °C, simply by extending the catalyst bed length to 7.5 cm. From an industrial point of view, extending catalyst bed lengths and utilising lower methanol WHSV may be an attractive way of achieving higher single-pass methanol conversions while keeping the reaction temperature, and thus the energy requirements, low. SAPOs undergo parallel deactivation whereby the deactivation front moves downwards from the catalyst bed inlet to the outlet.[32,55] As such, extending the catalyst bed can additionally reduce downtime associated with catalyst regeneration as longer beds will be able to tolerate prolonged deactivation before exhibiting an appreciable decline in outlet DME yields. A correlation matrix was also generated, seen in Table S10,† showcasing the influence of the input parameters (bed length, WHSV, temperature) on simulated methanol conversions, with larger magnitudes indicating higher

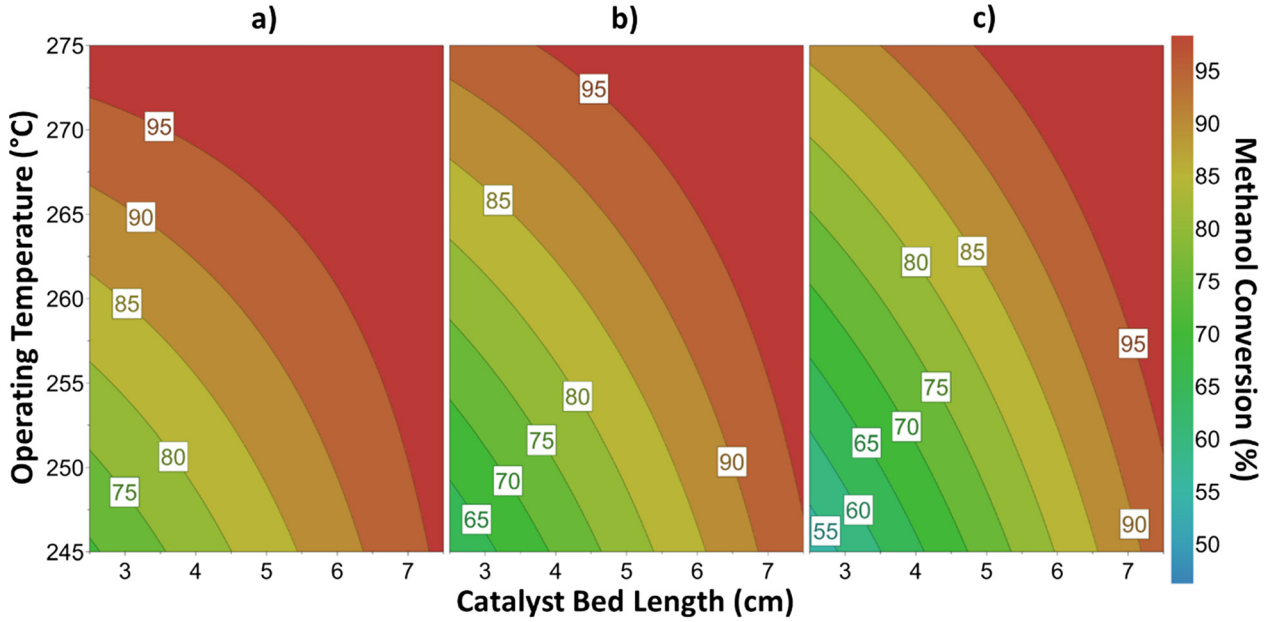

Fig. 7 Contour plots demonstrating the influence of reaction temperature and catalyst bed length on methanol conversion during the simulated methanol dehydration reaction over a SAPO-11 catalyst at a methanol weight hourly space velocity of a) 4 h^{-1} b) 5 h^{-1} and c) 6 h^{-1}.

influence, and the sign indicating either positive or negative influence. Thus, Table S10† demonstrates that the catalyst bed length (0.67) has a stronger impact on predicted methanol conversion than temperature (0.59), which further vindicates that optimising catalyst bed length is a better strategy to consider for larger scale pilot plant trials than increasing temperature as this can improve both conversions and catalyst longevity. Methanol WHSV has a deleterious (−0.22) influence on conversion for reasons already discussed.

A pure methanol feedstock was used for the experimental conversion of methanol-to-DME, and so our computational models are also based on a reactant feedstock free of contaminants. On an industrial scale, it is possible that the reaction feedstock will contain poisons such as sulphur or chlorine which can bind irreversibly to the catalyst and cause premature deactivation. Water, which can also be present in an industrial feedstock, can compete with methanol for the acidic active sites, and thus reduce the observed catalytic activity. If present in high quantities as an impurity in the methanol feedstock, water can additionally negatively influence the thermodynamic equilibrium as it is one of the reaction products, thus reducing single pass conversions.[56,57] With this in mind, to maintain efficient and stable production of DME on an industrial scale, pre-treatment of the methanol feedstock will be required to remove any contaminants.

Kyrimis *et al.* have previously calculated that a CFD-optimised reactor could achieve lower pressure drops and higher productivity during methanol synthesis compared to a baseline reactor,[30] demonstrating the ability of CFD to inform engineering decisions. Our CFD model could thus be used to inform larger scale pilot plant trials. Insights obtained from these trials, such as thermal management and reactor configuration constraints, could be fed back into our CFD model, further refining it. Combined with pilot plant trial data, the refined model could be used to support full commercialisation of the process. Given that the MTO reaction has been successfully commercialised over H-ZSM-5 and SAPO-34 catalysts, commercialisation of SAPO-11 for the sustainable production of DME is highly feasible and CFD models such as ours could be used to support this endeavour.

It is thus clear that CFD not only provides unique and complementary information to support experimental studies but can also be used to simulate reactions and rapidly screen different scenarios to gain knowledge which can be used to proactively design improved and energy efficient reactions, such as methanol dehydration over SAPO-11. Our developed modelling tools offer a valuable and accurate insight both for the fundamental understanding of the MTD reaction, and for the industrial practises necessary to optimise and scale-up this process. As discussed in Kyrimis *et al.*,[30] optimisation of industrial processes can substantially support the transition towards carbon neutral fuels which is necessary in achieving ambitious climate strategies.

Conclusions

Substituting fossil fuels with sustainable alternatives, such as DME, will increase the likelihood of meeting ambitious net-zero targets for the marine sector by 2050. In this vein, we investigated selective methanol dehydration to DME over SAPO-11 catalysts at a range of experimental conditions, to develop and validate a novel CFD model that can be used to inform scale up endeavours. We found an inverse correlation between experimental methanol conversion and methanol

inlet concentration and attributed this to a saturation of the SAPO-11 catalyst bed. Increasing the number of acid sites in SAPO-11 did increase experimental methanol conversions, but this approach was not trivial as it was difficult to substitute silicon into the SAPO-11 frameworks at high loadings. Increasing the SAPO-11 catalyst bed length was found to have the most beneficial influence on improving simulated single-pass conversions, and thus should be the strategy of choice for increasing yields and catalyst longevity while maintaining low reaction temperatures. Highest stability was achieved using smaller SAPO-11 granules due to limited residence time inside the granule, and lower methanol inlet concentrations. Combined, our experimental and computational investigation has shown that for industrial applications, using long catalyst beds comprised of small SAPO-11 granules and low inlet methanol concentrations will give highest single-pass methanol conversions and good time-on-stream stability.

Data availability

Data for this article, including raw characterisation and catalysis data, are available from the University of Southampton repository at **https://doi.org/10.5258/SOTON/D3366**.

Author contributions

MGW wrote the manuscript, performed the experimental work and kinetic calculations, and assisted with the CFD and DoE study. SK helped to write the manuscript, assisted with the kinetic calculations, and performed the CFD and DoE study. MEP collected the NH_3-TPD data, helped with the experimental design, and reviewed the manuscript. AEO and MC helped in the collection and analysis of the ssNMR data. LMA and RR helped with the study design, funding acquisition, supervision, and reviewing and editing of the manuscript. All authors have approved and contributed to the final manuscript.

Conflicts of interest

There are no conflicts to declare.

Acknowledgements

The project team would like to thank the University of Southampton, the Southampton Marine and Maritime Institute, and the Industrial Decarbonisation Research and Innovation Centre for funding. London Metropolitan University Elemental Analysis Service are thanked for the CHN analysis.

Notes and references

1 *International shipping - IEA*, **https://www.iea.org/energy-system/transport/international-shipping**, (accessed 7 September 2024).
2 Emissions-free sailing is full steam ahead for ocean-going shipping, **https://ec.europa.eu/research-and-innovation/en/horizon-magazine/emissions-free-sailing-full-steam-ahead-ocean-going-shipping**, (accessed 29 August 2023).
3 The Royal Society, *Sustainable synthetic carbon based fuels for transport: Policy briefing*, 2019.
4 S. J. Davis, N. S. Lewis, M. Shaner, S. Aggarwal, D. Arent, I. L. Azevedo, S. M. Benson, T. Bradley, J. Brouwer, Y. M. Chiang, C. T. M. Clack, A. Cohen, S. Doig, J. Edmonds, P. Fennell, C. B. Field, B. Hannegan, B. M. Hodge, M. I. Hoffert, E. Ingersoll, P. Jaramillo, K. S. Lackner, K. J. Mach, M. Mastrandrea, J. Ogden, P. F. Peterson, D. L. Sanchez, D. Sperling, J. Stagner, J. E. Trancik, C. J. Yang and K. Caldeira, *Science*, 2018, **360**, 1–9.
5 R. Schäppi, D. Rutz, F. Dähler, A. Muroyama, P. Haueter, J. Lilliestam, A. Patt, P. Furler and A. Steinfeld, *Nature*, 2022, **601**, 63–68.
6 A. Al-Enazi, E. C. Okonkwo, Y. Bicer and T. Al-Ansari, *Energy Rep.*, 2021, **7**, 1962–1985.
7 H. Stančin, H. Mikulčić, X. Wang and N. Duić, *Renew. Sustain. Energy Rev.*, 2020, **128**, 109927.
8 P. Balcombe, J. Brierley, C. Lewis, L. Skatvedt, J. Speirs, A. Hawkes and I. Staffell, *Energy Convers. Manage.*, 2019, **182**, 72–88.
9 J. Sun, G. Yang, Y. Yoneyama and N. Tsubaki, *ACS Catal.*, 2014, **4**, 3346–3356.
10 A. Álvarez, A. Bansode, A. Urakawa, A. V. Bavykina, T. A. Wezendonk, M. Makkee, J. Gascon and F. Kapteijn, *Chem. Rev.*, 2017, **117**, 9804–9838.
11 G. A. Olah, A. Goeppert and G. K. S. Prakash, *J. Org. Chem.*, 2009, **74**, 487–498.
12 A. Ghosh, D. Nag, R. Chatterjee, A. Singha, P. S. Dash, B. Choudhury and A. Bhaumik, *Catal. Sci. Technol.*, 2024, **14**, 1387–1427.
13 M. G. Walerowski, S. Kyrimis, V. A. Hewitt, L. M. Armstrong and R. Raja, *Chem. Commun.*, 2024, **60**, 10314–10317.
14 Z. Azizi, M. Rezaeimanesh, T. Tohidian and M. R. Rahimpour, *Chem. Eng. Process.: Process Intensif.*, 2014, **82**, 150–172.
15 H. Bateni and C. Able, *Catal. Ind.*, 2019, **11**, 7–33.
16 P. Yan, H. Peng, J. Vogrin, H. Rabiee and Z. Zhu, *J. Mater. Chem. A*, 2023, **11**, 17938–17960.
17 U. Olsbye, S. Svelle, M. Bjrgen, P. Beato, T. V. W. Janssens, F. Joensen, S. Bordiga and K. P. Lillerud, *Angew. Chem., Int. Ed.*, 2012, **51**, 5810–5831.
18 M. E. Potter, *ACS Catal.*, 2020, **10**, 9758–9789.
19 R. Raja, M. E. Potter and S. H. Newland, *Chem. Commun.*, 2014, **50**, 5940–5957.
20 J. Chen, P. A. Wright, J. M. Thomas, S. Natarajan, L. Marchese, S. M. Bradley, G. Sankar, C. Richard, A. Catlow, P. L. Gai-Boyes, R. P. Townsend and C. M. Lok, *J. Phys. Chem.*, 1994, **98**, 10217.
21 S. Chapman, M. E. Potter and R. Raja, *Molecules*, 2017, **22**, 2127.
22 W. Dai, W. Kong, G. Wu, N. Li, L. Li and N. Guan, *Catal. Commun.*, 2011, **12**, 535–538.

23 A. K. Sinha and S. Seelan, *Appl. Catal., A*, 2004, **270**, 245–252.
24 P. Liu, J. Ren and Y. Sun, *Microporous Mesoporous Mater.*, 2008, **114**, 365–372.
25 M. R. Agliullin, Y. G. Kolyagin, D. V. Serebrennikov, N. G. Grigor'eva, A. S. Dmitrenok, V. N. Maistrenko, E. Dib, S. Mintova and B. I. Kutepov, *Microporous Mesoporous Mater.*, 2022, **338**, 111962.
26 P. Mériaudeau, V. A. Tuan, V. T. Nghiem, S. Y. Lai, L. N. Hung and C. Naccache, *J. Catal.*, 1997, **169**, 55–66.
27 S. Lin, Y. Zhi, W. Chen, H. Li, W. Zhang, C. Lou, X. Wu, S. Zeng, S. Xu, J. Xiao, A. Zheng, Y. Wei and Z. Liu, *J. Am. Chem. Soc.*, 2021, **143**, 12038–12052.
28 E. Catizzone, A. Aloise, M. Migliori and G. Giordano, *Microporous Mesoporous Mater.*, 2017, **243**, 102–111.
29 *ANSYS Fluent Theory Guide 15*, ANSYS, Inc., Canonsburg, 2013.
30 S. Kyrimis, R. Raja and L. M. Armstrong, *Fuel*, 2024, **368**, 131511.
31 M. E. Potter, L. M. Armstrong and R. Raja, *Catal. Sci. Technol.*, 2018, **8**, 6163–6172.
32 Y. Q. Zhuang, X. Gao, Y. p. Zhu and Z. h. Luo, *Powder Technol.*, 2012, **221**, 419–430.
33 S. Kyrimis, M. E. Potter, R. Raja and L. M. Armstrong, *Faraday Discuss.*, 2021, **230**, 100–123.
34 K. V. V. S. B. S. R. Murthy, S. J. Kulkarni and S. K. Masthan, *Microporous Mesoporous Mater.*, 2001, **43**, 201–209.
35 I. Grenev, N. D. Klimkin, I. A. Shamanaeva, A. A. Shubin, I. A. Chetyrin and V. Y. Gavrilov, *Microporous Mesoporous Mater.*, 2021, **328**, 111503.
36 M. G. Walerowski, M. E. Potter, E. S. Burke, S. Kyrimis, L. M. Armstrong and R. Raja, *Catal. Sci. Technol.*, 2024, **14**, 3853–3863.
37 S. Kyrimis, K. E. Rankin, M. E. Potter, R. Raja and L. M. Armstrong, *Adv. Powder Technol.*, 2023, **34**, 103932.
38 S. K. Wilkinson, L. G. A. Van De Water, B. Miller, M. J. H. Simmons, E. H. Stitt and M. J. Watson, *J. Catal.*, 2016, **337**, 208–220.
39 S. Hoops, R. Gauges, C. Lee, J. Pahle, N. Simus, M. Singhal, L. Xu, P. Mendes and U. Kummer, *Bioinformatics*, 2006, **22**, 3067–3074.
40 Z. Michalewicz, *Genetic Algorithms + Data Structures = Evolution Programs*, Springer, Berlin Heidelberg, 1996.
41 K. Levenberg and F. Arsenal, *Q. Appl. Math.*, 1944, **2**, 164–168.
42 D. W. Marquardt, *J. Soc. Ind. Appl. Math.*, 1963, **11**, 431–441.
43 *Ansys Fluent*, **https://www.ansys.com/**, (accessed 19 November 2024).
44 S. Ergun, *Chem. Eng. Prog.*, 1952, **48**, 89–94.
45 A. De Klerk, *AIChE J.*, 2003, **49**, 2022–2029.
46 *Sartorius MODDE*, **https://www.sartorius.com/en/products/process-analytical-technology/data-analytics-software/doe-software/modde**, (accessed 19 November 2024).
47 C. H. Bartholomew and R. J. Farrauto, *Fundamentals Of Industrial Catalytic Processes*, Wiley-Interscience, 2nd edn, 2006.
48 G. Pop, G. Bozga, R. Ganea and N. Natu, *Ind. Eng. Chem. Res.*, 2009, **48**, 7065–7071.
49 E. Catizzone, A. Aloise, M. Migliori and G. Giordano, *Appl. Catal., A*, 2015, **502**, 215–220.
50 J. M. Campelo, F. Lafont, J. M. Marinas and M. Ojeda, *Appl. Catal., A*, 2000, **192**, 85–96.
51 W. Dai, G. Wu, L. Li, N. Guan and M. Hunger, *ACS Catal.*, 2013, **3**, 588–596.
52 W. Dai, X. Wang, G. Wu, N. Guan, M. Hunger and L. Li, *ACS Catal.*, 2011, **1**, 292–299.
53 E. Catizzone, E. Giglio, M. Migliori, P. C. Cozzucoli and G. Giordano, *Materials*, 2020, **13**, 5577.
54 J. R. Di Iorio, A. J. Hoffman, C. T. Nimlos, S. Nystrom, D. Hibbitts and R. Gounder, *J. Catal.*, 2019, **380**, 161–177.
55 J. J. Birtill, *Catal. Today*, 2003, **81**, 531–545.
56 S. S. Akarmazyan, P. Panagiotopoulou, A. Kambolis, C. Papadopoulou and D. I. Kondarides, *Appl. Catal., B*, 2014, **145**, 136–148.
57 S. Hosseininejad, A. Afacan and R. E. Hayes, *Chem. Eng. Res. Des.*, 2012, **90**, 825–833.